ELSEVIER

Journal of Nuclear Materials 294 (2001) 267–273

journal of nuclear materials

www.elsevier.nl/locate/jnucmat

Numerical simulation modeling on the effects of grain boundary misorientation on radiation-induced solute segregation in 304 austenitic stainless steels

T.S. Duh, J.J. Kai *, F.R. Chen, L.H. Wang

Center for Electron Microscopy, Department of Engineering and System Science, National Tsing Hua University, 101 Section II, Kuang-fu Road, Hsin-chu 300, Taiwan, ROC

Received 6 November 2000; accepted 20 January 2001

Abstract

The purpose of this study is to develop a model to describe the effects of the grain boundary misorientation on the radiation-induced solute segregation (RIS) in 304 stainless steels. A simple rate equation model with modified boundary conditions, which included the fluxes of defects diffusing along the grain boundaries to the grain boundary dislocations, was developed for RIS at boundaries with different Σ values. The results of the model calculations were compared to the experimental results previously reported by us. It was found that the model could clearly predict the same trends that the Cr depletion levels at special boundaries in irradiated 304 stainless steels were increasing with Σ. The model calculations also showed that the widths of the segregation cusps was decreasing with increasing Σ.

1. Introduction

The mechanisms of the radiation-induced solute segregation (RIS) may be described by inverse-Kirkendall models [1]. During irradiation, defect fluxes are generated and a gradient in defect concentration may result in a net flux of alloy components across a lattice plane. Hence, the radiation-induced defect fluxes can induce compositional gradients in initially homogeneous alloy. Normally, it is assumed that the grain boundaries are perfect sinks, and therefore the boundary condition for defect concentrations at the grain boundaries may be taken as equal to the thermal equilibrium defect concentrations. However, in real situation, the actual boundaries, for instance the $\Sigma = 3$ boundaries, would not always behave like perfect sinks [2]. The defect concentrations at the grain boundaries will generally depend both upon how rapidly the flux of defects can be absorbed at the boundaries and how fast the flux of defects can diffuse to the grain boundaries.

It is well known that the interfaces can be modeled by continuously or discretely distributed arrays of dislocations [3,4]. For low-angle boundaries the mechanism available for the absorption of the point defects is the climbing of the primary dislocations in the boundaries. The point defects are absorbed at jogs on the climbing dislocations by means of thermally activated fluctuations [5]. However, for singular or vicinal high-angle boundaries, the absorption of the point defects at boundaries is more readily via the climb of the secondary dislocations [6], due to the facts that such boundaries with reference structures of low energy are resistant to the simultaneous climb of their primary dislocations. Normally, the diffusing defects from the bulk will impinge upon the boundary surface and then diffuse along the grain boundary to the grain boundary dislocations, and furthermore, diffuse along the cores of grain boundary dislocations to the jogs where the defects absorbed [7].

In this study we consider the effects of the grain boundary diffusion on RIS. A rate equation model with

* Corresponding author. Tel.: +886-3 574 2855; fax: +886-3 571 6770.

E-mail address: jjkai@ess.nthu.edu.tw (J.J. Kai).

0022-3115/01/$ - see front matter
PII: S0022-3115(01)00493-7

modified boundary conditions, which include the flux of defects diffusing along the grain boundaries to the grain boundary dislocations, is developed for RIS at boundaries of different Σ values (where Σ is the reciprocal density of coincidence sites). The model is compared to the experimental data from our previous work [8] which showed that the Cr depletion levels at special boundaries in irradiated 304 stainless steels could be obtained with different Σ values and misorientation.

2. Model description

The RIS model used here for Fe–Cr–Ni alloys is based on the Lam et al.'s model [9] which is based on the concept of preferential migration of defects via atoms of the constituent elements and preferential defect–atom association. The rate equations of atoms (Fe, Cr and Ni) and defects (vacancy and interstitial) are

$$\begin{aligned}
\frac{\partial C_{\mathrm{v}}}{\partial t} &= -\nabla\cdot\Omega J_{\mathrm{v}} + \eta K_0 - RC_{\mathrm{v}}C_{\mathrm{i}},\\
\frac{\partial C_{\mathrm{i}}}{\partial t} &= -\nabla\cdot\Omega J_{\mathrm{i}} + \eta K_0 - RC_{\mathrm{v}}C_{\mathrm{i}},\\
\frac{\partial C_{\mathrm{k}}}{\partial t} &= -\nabla\cdot\Omega J_{\mathrm{k}} \quad (\mathrm{k} = \mathrm{Cr},\ \mathrm{Ni\ or\ Fe}).
\end{aligned} \tag{1}$$

C_{k}s are the fractions of atoms, and C_{v} and C_{i} are the fractions of vacancies and interstitials, respectively. Ω, R and ηK_0 are the atomic volume, the recombination coefficient and the effective damage rate, respectively. The fluxes of the defects and atoms can be written as the form

$$\begin{aligned}
J_{\mathrm{v}} &= J_{\mathrm{v}}^{\mathrm{Cr}} + J_{\mathrm{v}}^{\mathrm{Ni}} + J_{\mathrm{v}}^{\mathrm{Fe}},\\
J_{\mathrm{i}} &= J_{\mathrm{i}}^{\mathrm{Cr}} + J_{\mathrm{i}}^{\mathrm{Ni}} + J_{\mathrm{i}}^{\mathrm{Fe}},\\
J_{\mathrm{k}} &= J_{\mathrm{k}}^{\mathrm{v}} + J_{\mathrm{k}}^{\mathrm{i}},\\
J_{\mathrm{v}}^{\mathrm{k}}(\equiv -J_{\mathrm{k}}^{\mathrm{v}}) &= d_{\mathrm{vk}}(C_{\mathrm{v}}\alpha\nabla C_{\mathrm{k}} - C_{\mathrm{k}}\nabla C_{\mathrm{v}})/\Omega,\\
J_{\mathrm{i}}^{\mathrm{k}}(\equiv J_{\mathrm{k}}^{\mathrm{i}}) &= d_{\mathrm{ik}}(-C_{\mathrm{i}}\alpha\nabla C_{\mathrm{k}} - C_{\mathrm{k}}\nabla C_{\mathrm{i}})/\Omega,
\end{aligned} \tag{2}$$

where $J_{\mathrm{v}}^{\mathrm{k}}(J_{\mathrm{i}}^{\mathrm{k}})$ is the partial vacancy (interstitial) flux via k atoms, and $J_{\mathrm{k}}^{\mathrm{v}}(J_{\mathrm{k}}^{\mathrm{i}})$ is the partial flux of k atoms via vacancies (interstitials). α and d_{jk} (j = v or i) are the thermodynamic factor and the diffusivity coefficients for defect–atom pairs jk, respectively. Usually, the initial conditions are:

(a) thermal equilibrium defect concentrations;
(b) uniform composition of the alloy throughout.

The boundary conditions at the grain boundaries for the atoms are $J_{\mathrm{k}} = 0$ because of conservation of atoms in a closed system, and for the defects are generally taken as equal to the thermal equilibrium concentrations if the grain boundaries are perfect sinks. For actual grain boundaries, however, the thermal equilibrium defects concentrations may not be maintained in their vicinities due to the lower sink efficiency of the boundaries. The boundary conditions for defects at normal boundaries will be modified here.

We will consider, for simplicity, a pure symmetric tilt boundary consisting of an array of parallel edge dislocations, which are primary dislocations for low-angle boundary or secondary dislocations for singular or vicinal high-angle boundary, and assume that these grain boundary dislocations are perfect sinks for defects. The rate equations for vacancies in a region of the lattice directly adjacent to the boundary, as shown in Fig. 1, may be written as

$$\Delta x\frac{\partial C_{\mathrm{v}}}{\partial t} = \Omega J_{\mathrm{v}}^{1} - \Omega J_{\mathrm{v}}^{0} + \Delta x\,\eta K_0 - \Delta x RC_{\mathrm{v}}C_{\mathrm{i}}, \tag{3}$$

where J_{v}^{1} and J_{v}^{0} are the fluxes of vacancies flowing into and out of the region directly adjacent to the boundary, respectively. The vacancies leaving the directly vicinal region, for high-angle boundary, are assumed to diffuse along the grain boundary to the secondary grain boundary dislocations, and for low-angle boundary are assumed to diffuse directly to the primary grain boundary dislocations. The grain boundary dislocations, due to assumed to be perfect sinks, can maintain the concentration of defects in its direct vicinity at its local equilibrium value, $C_{\mathrm{v}}^{\mathrm{eq}}$. The flux J_{v}^{0} may be related to the flux along the boundary, $J_{\mathrm{v}}^{\mathrm{gb}}$, by

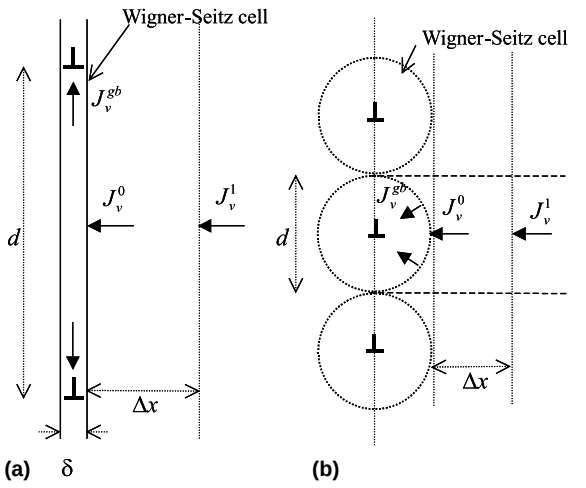

Fig. 1. Diagrams of modified boundary conditions for defects at grain boundaries in RIS model. (a) The defects impinging upon the high-angle grain boundaries through a cross-section of $1 \times d$ will diffuse along boundaries through a cross-section of $1 \times \delta$ to dislocations where defects absorbed. (b) The defects will diffuse directly to the grain boundary dislocations in low-angle boundaries.

$$J_v^0 1d = 2J_v^{gb} 1\delta \quad \text{(for high-angle GB, and } J_v^{gb} \text{ in } 1/\text{cm}^2\text{)}, \tag{4a}$$

$$J_v^0 1d = J_v^{gb} \times 1 \quad \text{(for low-angle GB, and } J_v^{gb} \text{ in } 1/\text{cm}\text{)}, \tag{4b}$$

where d and δ are the distance between grain boundary dislocations and boundary thickness, respectively. For low-angle grain boundary, J_v^{gb} on the right-hand side of Eq. (4b) is defined as a flux flowing into per unit length of dislocation line and is in units of 1/cm. The number 1 in Eqs. (4a) and (4b) means the unit width we take in grain boundary. Since the vacancies can jump via Fe, Cr or Ni in the boundary, the vacancy flux along boundary can be written as

$$J_v^{gb} = \sum J_{vk}^{gb} \quad (k = \text{Fe, Cr and Ni}), \tag{5}$$

where J_{vk}^{gb} is the flux of vacancies via k atoms in the boundary. J_{vk}^{gb} is assumed to have the form as

$$\Omega J_{vk}^{gb} = S d_{vk}^{gb} C_k (C_v - C_v^{eq}), \tag{6}$$

where S is the sink strength of the grain boundary dislocations and d_{vk}^{gb} is the diffusivity coefficients for vacancy–atom pairs vk in the boundary. The sink strength S may be written as a product of three parameters [7], in the form

$$S = g_0 z m, \tag{7}$$

where g_0 is a purely geometrical parameter, z is the sink capture efficiency and m is a multiple sink correction factor. The geometrical parameter, g_0, for the sink of grain boundary dislocations is $g_0 = 1/(d/2 - r_0)$ for high-angle boundaries and $g_0 = \pi/\ln(d/2r_0)$ for low-angle boundaries [7], r_0 is the radius of the grain boundary dislocations, here we set $r_0 = \alpha b$, b is the Burgers vector of grain boundary dislocation and α is a constant of the order of unity [6]. The parameter z is defined as the ratio of the actual point defect current to the sink to the corresponding current which would result if the sink were perfect. In our case, $z = 1$ for grain boundary dislocations which are assumed to be perfect sinks. The parameter m accounts for the interactions between sinks when many sinks are present. We will ignore the interactions between grain boundary dislocations, so $m = 1$ here. The diffusivity coefficients in the boundaries may be written as [6]

$$d_{vk}^{gb} = g_v a^2 Z_v f_v^{gb} (\nu_{vk})_0 \exp\left(-\frac{E_{vk}^m}{kT}\right). \tag{8}$$

Here, g_v is a dimensionless constant depending on the structure, a the lattice constant, Z_v the coordination number, f_v^{gb} the correlation factor, $(\nu_{vk})_o$ the vibrational frequency (including entropy term), and E_{vk}^m is the migration energy for diffusion of a vacancy via k atom in the boundaries. We assume that $(\nu_{vk})_o$ in the boundaries have the same values as that in the bulk, and take $f_v^{gb} = 0.5$ [10]. If the energies of the activated state in diffusion are approximately the same for the boundary and bulk, the migration energies of the grain boundary and bulk diffusion may be related to grain boundary energy (γ) by the expression [11]

$$E_{vk}^m \approx E_{vk,bulk}^m - \frac{a^2}{n}\gamma, \tag{9}$$

where a is the lattice constant and n is the thickness of a boundary expressed in terms of the number of atomic layers. We will take $n = 1$ here [12].

Based on the grain boundary dislocation model, the grain boundary energy can be written as [13]

$$\gamma = \gamma_0 + \gamma_{core} + \gamma_{el}, \tag{10}$$

where γ_0 is the energy per unit area of the reference structure, γ_{core} is the core energy of the grain boundary dislocations per unit area of the boundary and γ_{el} is the elastic energy per unit area of the boundary associated with the elastic field of the grain boundary dislocations. In general, the core and the elastic energies of the dislocations are mainly confined to the dislocations themselves. For the boundaries with small deviations from CSL, the boundary energies of the regions in between grain boundary dislocations are mostly γ_0. In our model, we will focus on the segregation effects of special boundaries, and besides the diffusion we concern occurs mainly on the area of the reference structure, therefore, for simplicity we will assume that the energy of grain boundary is mainly from that of the reference structure, γ_0, and ignore the core and elastic energies of grain boundary dislocations in Eq. (10). In CSL model, the boundaries with lower Σ value have better matching structure than those with higher Σ value. It was shown in [14], and will be adopted here, that the grain boundary energy could be related to Σ by the following expression on the basis of the coincidence site concept:

$$\gamma = \gamma_b\left(1 - \frac{1}{\sqrt{\Sigma}}\right). \tag{11}$$

Here, γ_b is the energy of 'bad' boundaries. The similar assumptions were also adopted by Morawiec [18] in his calculation of distribution of grain boundary energy over grain misorientation in which the energy depths were determined by $\Sigma^{-1/2}$. Substituting Eq. (11) into Eq. (9), we obtain

$$E_{vk}^m \approx E_{vk,bulk}^m - \frac{a^2}{n}\gamma_b\left(1 - \frac{1}{\sqrt{\Sigma}}\right). \tag{12}$$

Back to Eqs. (4a) and (4b), the boundary conditions for the flux of vacancies at grain boundaries can be rewritten as

$$J_v^0 = 2J_v^{gb}\delta\frac{b}{d}\frac{1}{b} = 2J_v^{gb}\delta\frac{2}{b}\sin(\Delta\theta/2)$$
(for high-angle GB), (13a)

$$J_v^0 = J_v^{gb}\frac{b}{d}\frac{1}{b} = J_v^{gb}\frac{2}{b}(\theta/2)$$
(for low-angle GB), (13b)

where, in Eq. (13a), b is the Burgers vector of the secondary grain boundary dislocations and $\Delta\theta$ is the deviation angle from exact CSL boundary ($\Delta\theta = \theta - \theta_{CSL}$), and in Eq. (13b), b is the Burgers vector of the primary grain boundary dislocations and θ is the misorientation angle. For high-angle boundary, the reference lattice of the grain boundary is a DSC-Lattice in which the lattice spacing may be equal, or approximately close to $a/\sqrt{\Sigma}$. Hence, the length of Burgers vectors of the secondary grain boundary dislocations in Σ-boundary may be approximately taken as $a/\sqrt{\Sigma}$. Similarly, the boundary conditions for the flux of interstitials at grain boundaries can be obtained.

3. Model results and discussion

The calculations were performed to evaluate the segregation levels of solute atoms at grain boundaries of different Σ values. The LSODE numerical integration subroutine was used for the rate equations. The input parameters for rate equations were assumed to be the same as used by Allen et al. [15] and were listed in Table 1. So far, the yet determined parameter is the grain boundary energy, γ_b, in Eq. (11), and it could be determined from measured free energies of grain boundaries of $\Sigma = 3$. The reason for not choosing measured energies of general boundaries in determining γ_b is that the energies of general boundaries are generally composed of γ_0, γ_{core} and γ_{el}, and as mentioned above it is γ_0 that we need in this model calculations. The measured free energies [16] of grain boundaries in 304 stainless steels were 19 erg/cm^2 for coherent twin boundaries, and 209 erg/cm^2 for non-coherent twin boundaries, and these values were taken at a temperature of 1060°C. The experimentally determined dependence of grain boundary free energy with temperature was a linear relationship with a temperature coefficient −0.12 erg/cm^2 K for non-coherent twin boundaries in 304 stainless steels. Hence, the grain boundary energies of non-coherent boundaries would be about 336 erg/cm^2 provided that the linear relationship of grain boundary free energy with temperature was held at low temperatures. From the experimental data in hand, we cannot exactly determine the grain boundary energies of $\Sigma = 3$, because these energies may be dependent upon the degree of coherence of the boundaries. However, we can, at least, tell the range where they lie, i.e., somewhere between 20 and 336 erg/cm^2. Here, we will arbitrarily take a value for the grain boundary energy, γ_0, of $\Sigma = 3$ in 304 stainless steels, say 150 erg/cm^2. Substituting this value into Eq. (11), we obtain $\gamma_b = 355$ erg/cm^2.

Fig. 2 shows the variations in Cr segregation levels at grain boundaries of different Σ values as a function of misorientation angles for sensitized irradiated 304 stainless steels. In Fig. 2, model calculations were compared with the experimental data [8] which came with the sensitized 304 specimens irradiated by protons up to a dose of 1 dpa with damage rates 1×10^{-6} dpa/s at an irradiation temperature of 450°C. In order to compare with the measured composition profiles, we have taken into account the beam broadening effect by a convolution of the calculated composition profile with the X-ray generation function which was coming with the broadened electron beam. Both of the calculated and measured results indicate the trends that the Cr segregation levels at special boundaries (here, special boundaries

Table 1
RIS input parameters in this model

Input parameter	Notation	Value	Refs.
Vacancy jump frequency for Fe	ν^0_{Fe-v}	2.8×10^{13} 1/s	[19]
Vacancy jump frequency for Cr	ν^0_{Cr-v}	5.0×10^{13} 1/s	[19]
Vacancy jump frequency for Ni	ν^0_{Ni-v}	1.5×10^{13} 1/s	[19]
Interstitial jump frequency for Fe, Cr and Ni	ν^0_{k-i}	1.5×10^{12} 1/s	[20]
Vacancy migration energy for Fe, Cr and Ni	H^m_{k-v}	1.3 eV	[21]
Interstitial migration energy for Fe, Cr and Ni	H^m_{k-i}	0.9 eV	[22]
Vacancy formation energy	H^f_v	1.9 eV	[9]
Interstitial formation energy	H^f_i	4 eV	[24]
Fe-vacancy correlation factor	f_{Fev}	0.785	[19]
Cr-vacancy correlation factor	f_{Crv}	0.668	[19]
Ni-vacancy correlation factor	f_{Niv}	0.872	[19]
Atom-interstitial correlation factor	f_I	0.44	[23]
Vacancy formation entropy	S^f_v	$5k$	[24]
Interstitial formation entropy	S^f_i	$0k$	[24]

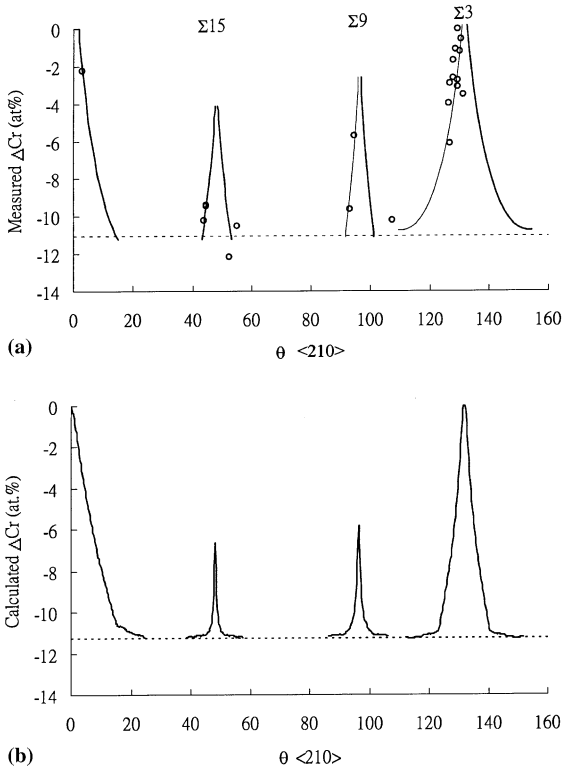

Fig. 2. The variations in Cr segregation levels at grain boundaries of different Σ value as a function of misorientation angles with rotation axis $\langle 210 \rangle$ for sensitized irradiated 304 stainless steels. Both of the (a) measured and (b) calculated results indicate the trends that the Cr segregation levels at special boundaries are increasing with Σ.

mean vicinal or singular boundaries) in irradiated 304 stainless steels are increasing with Σ for the lower Σ values. Although not obvious, we can see in Fig. 2 that the widths of the cusps also change with the Σ values as implied by the Brandon criterion [17]. In doing the above model calculations for the sensitized irradiated case, the measured sensitized concentration profiles were taken as the initial profiles for $\Sigma = 9$ and 15 boundaries, but for low-angle and $\Sigma = 3$ boundaries the depths and widths of initial profiles were assumed to be increasing with misorientation angles. In this model, the segregation levels are estimated to be equal to zero at singular boundaries, so the segregation levels in Fig. 2 were estimated at vicinal boundaries with $\Delta\theta = 0.1°$.

Fig. 3 plots the predicted segregation levels of Cr at boundaries at different temperatures for as-received 304 stainless steels with 1 dpa irradiation. It can be also seen that the calculated segregation levels of Cr at grain boundaries are increasing with Σ for boundaries with the same initial concentrations which were uniformly distributed over the bulk in as-received 304 stainless steels. At elevated temperatures, seen from

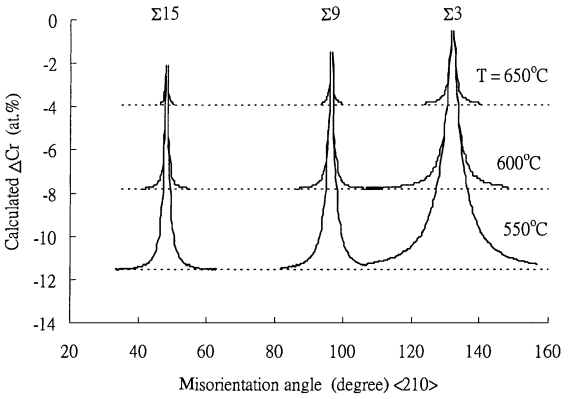

Fig. 3. Variations of the predicted Cr segregation levels for boundaries at different temperatures for as-received 304 stainless steels with 1 dpa irradiation.

Fig. 3, the segregation levels decrease and the cusps disappear gradually when temperature increases. The causes for these are:

(a) fast back-diffusion of solute atoms and high recombination rate of radiation-induced defects with thermal vacancies;

(b) smaller boundary energy effects (i.e., $\exp(\gamma/kT)$ getting smaller) at high temperatures.

The similar situation can be seen from the plots of the grain boundary energy vs. temperature. The effect of increasing temperature will made cusps shallower and wider and shallow cusps will thus be lost at high temperatures [25].

At early times during irradiation, J_v^0 is approximately equal to zero because C_v at grain boundaries is close to C_v^{eq} in Eq. (6). As time goes on, J_v^0 along with C_v is increasing with time till $\partial C_v/\partial t = 0$. At steady state, J_v^0 is balanced off by the rest terms, $J_v^1 + (\eta K_0 - RC_vC_i)\Delta X/\Omega$, on the right-hand side of Eq. (3). Hence, the equilibrium defect concentrations at grain boundaries may be determined from Eqs. (3) and (6) at steady state. For general boundaries, the diffusivity coefficient, d_{vk}^{gb}, in boundaries is a very large value compared to that in bulk, for instance, for grain boundary energy of 1 J/m^2 at 450°C $d_{vk}^{gb}/d_{vk} \approx 6.1 \times 10^5$. J_v^0 would become a large value due to a small increasing in C_v from C_v^{eq}, so that the general boundaries would absorb the defects very rapidly and behave as perfect sinks. In this model, therefore, for general boundaries the equilibrium defect concentration at steady state is very close to that in thermal equilibrium, and this is just the assumption mentioned above for general boundaries. For special boundaries, the diffusing fluxes on boundaries are smaller than those on general boundaries due to the facts that the energies of special boundaries are lower than those of general boundaries, and this can be expected from Eqs. (6), (8) and (9). To increase the

diffusing fluxes on special boundaries for reaching steady states, the defect concentrations at grain boundaries need to be higher than those at general boundaries. Therefore, the defect concentrations at special boundaries at steady state are higher than thermal equilibrium values, as can be seen from Eq. (6), and their values are dependent upon the energies of grain boundaries.

For low-angle boundaries, the degree of segregation increases with misorientation (θ), and this can be attributed to the increase in primary dislocation density with misorientation. For high-angle boundaries, the segregation cusps usually occur at special boundaries due to the facts that they have lower energy structures than general boundaries do. This phenomenon was also observed in the work of Watanabe et al. [26] in which the intergranular RIS was suppressed at low-sigma boundaries of $\Sigma 9$ and $\Sigma 3$ and a small angle grain boundary. When deviated from the exact CSL boundary, the segregation levels will also increase with the misorientation ($\Delta\theta = \theta - \theta_{CSL}$), and similarly this can also be attributed to the increase in the density of secondary grain boundary dislocations with misorientation. Besides, segregation levels will depend upon the magnitude of diffusing defect fluxes on boundaries which in turn depends upon the grain boundary energies. In our model, the Cr segregation levels at special boundaries will be increasing with Σ if we adopt the assumption that the grain boundary energy could be related to Σ by Eq. (11).

This model was shown to predict the radiation-induced segregation for grain boundaries of different energies and misorientation. However, there are some limitations in this model as described below. Some of the input parameters used on grain boundary, which are not available for this moment, were assumed to be the same as those used in bulk, and this may not be the truth. Especially, the grain boundary energies for special boundaries of different Σs in 304 stainless steels are not available from measurements or theoretical calculations, except $\Sigma 3$ boundaries. Dislocations were treated as ideal sinks for defect fluxes in this model. Actually, the absorption of defects at the dislocation lines is a complex process to Ref. [6] which involves the jumping of defects into the core, the diffusion of these defects along the core to jogs, and the nucleation of jog pairs. For further details on the sink efficiency of dislocations please refer to Ref. [6]. The elastic fields of dislocations and boundaries were also neglected in this model. They are local fields and confined to dislocations within the range of few Burgers vectors. When misorientation angle is small, the distance between grain boundary dislocations is large so that any effects of the stress field are relatively small and can be neglected. However, for large misorientation angle, the stress field may overlap each other and may not be negligible.

4. Summary

In this study, we have considered the effects of the grain boundary misorientation on RIS. A simple rate equation model with modified boundary conditions, which include the fluxes of defects diffusing along the grain boundaries to the grain boundary dislocations, is developed for RIS at boundaries of different Σ values. The results of the model calculations are summarized as follows:

1. If the relationship between grain boundary energy and Σ as expressed in Eq. (11) is adopted, the model calculations indicate the trends that the Cr depletion levels at special boundaries are increasing with Σ. This result agrees with that of our previous experiment which showed the same trend in sensitized irradiated 304 stainless steels.
2. The widths of the segregation cusps also change with the Σ values as implied by the Brandon criterion.
3. At elevated temperatures, the segregation levels decrease and the cusps disappear gradually when temperature increases.

Acknowledgements

This work was financially supported by the National Science Council of the Republic of China under contract number of NSC-89-2212-E-007-059.

References

[1] P.R. Okamoto, L.E. Rehn, J. Nucl. Mater. 83 (1979) 2.
[2] T.S. Duh, J.J. Kai, F.R. Chen, L.H. Wang, J. Nucl. Mater. 258–263 (1998) 2064.
[3] W.T. Read, Dislocations in Crystals, McGraw-Hill, New York, 1953.
[4] R.W. Balluffi, in: W.C. Johnson, J.M. Blakely (Eds.), Interfacial Segregation, American Society for Metals, Metals Park, OH, 1977, p. 193.
[5] R.W. Balluffi, Phys. Stat. Sol. 31 (1969) 443.
[6] A.P. Sutton, R.W. Balluffi, Interfaces in Crystalline Materials, Clarendon, Oxford, 1995.
[7] R.W. Balluffi, A.H. King, in: F.V. Nolfi Jr. (Ed.), Phase Transformation During Irradiation, Applied Science, London, 1983, p. 147.
[8] T.S. Duh, J.J. Kai, F.R. Chen, J. Nucl. Mater. 283 (2000) 198.
[9] N.Q. Lam, A. Kumar, H. Wiedersich, in: H.R. Brager, J.S. Perrin (Eds.), Effects of Radiation on Materials: Eleventh Conf., ASTM STP 782, American Society for Testing and Materials, 1982, p. 985.
[10] R.W. Balluffi, in: G.E. Murch, A.S. Nowick (Eds.), Diffusion in Crystalline Solids, Academic Press, Orlando, FL, 1984, p. 319.

[11] A.N. Aleshin, B.S. Bokshtein, L.S. Shvindlerman, Sov. Phys. Solid State 19 (12) (1977) 2051.
[12] V.T. Borisov, V.M. Golikov, G.V. Scherbedinskiy, Fiz. Met. Metalloved. 17 (6) (1964) 881.
[13] D. Schwartz, P.D. Bristowe, V. Vitek, Acta Metall. 36 (3) (1988) 675.
[14] A.N. Aleshin, V.Yu. Aristov, B.S. Bokshtein, L.S. Shvindlerman, Phys. Stat. Sol. (a) 45 (1978) 359.
[15] T.R. Allen, G.S. Was, E.A. Kenik, J. Nucl. Mater. 244 (1997) 278.
[16] L.E. Murr, Interfacial Phenomena in Metals and Alloys, Addison-Wesley, Reading, MA, 1975.
[17] D.G. Brandon, Acta Metall. 14 (1966) 1479.
[18] A. Morawiec, Scr. Mater. 41 (1) (1999) 13.
[19] S.J. Rothman, L.J. Nowicki, G.E. Murch, J. Phys. 10 (1980) 383.
[20] J.M. Perks, A.D. Marwick, C.A. English, A computer code to calculate radiation-induced segregation in concentrated ternary alloys, AERE Report R 12121, 1986.
[21] M. Kiritani, H. Takata, J. Nucl. Mater. 69–70 (1978) 277.
[22] C. Dimitrov, O. Dimitrov, J. Phys. F 14 (1984) 793.
[23] R.W. Seigel, in: J. Takamura, M. Doyama, M. Kiritani (Eds.), Point Defects and Defect Interactions in Metals, North-Holland, Amsterdam, 1982, p. 533.
[24] A.M. Yacout, N.Q. Lam, J.F. Stubbins, Nucl. Instrum. and Meth. B 42 (1989) 49.
[25] H.J. Frost, M.F. Ashby, F. Spaepen, Grain Boundary Structure and Kinetics, American Society for Metals, Metals Park, OH, 1980.
[26] S. Watanabe, Y. Takamatsu, N. Sakaguchi, H. Takahashi, J. Nucl. Mater. 283–287 (2000) 152.